ACS APPLIED MATERIALS & INTERFACES

Research Article

www.acsami.org

Toward Silicon Anodes for Next-Generation Lithium Ion Batteries: A Comparative Performance Study of Various Polymer Binders and Silicon Nanopowders

Christoph Erk,*[,†,‡] Torsten Brezesinski,[†] Heino Sommer,[†,‡] Reinhard Schneider,[§] and Jürgen Janek*[,†,⊥]

[†]Battery and Electrochemistry Laboratory, Institute of Nanotechnology, Karlsruhe Institute of Technology, Hermann-von-Helmholtz-Platz 1, 76344 Eggenstein-Leopoldshafen, Germany

[‡]BASF SE, 67056 Ludwigshafen, Germany

[§]Laboratory for Electron Microscopy, Karlsruhe Institute of Technology, Engesserstrasse 7, 76131 Karlsruhe, Germany

[⊥]Institute of Physical Chemistry, Justus-Liebig-University Giessen, Heinrich-Buff-Ring 58, 35392 Giessen, Germany

Supporting Information

ABSTRACT: Silicon is widely regarded as one of the most promising anode materials for lithium ion and next-generation lithium batteries because of its high theoretical specific capacity. However, major issues arise from the large volume changes during alloying with lithium. In recent years, much effort has been spent on preparing nanostructured silicon and optimizing various aspects of material processing with the goal of preserving the electrode integrity upon lithiation/delithiation. The performance of silicon anodes is known to depend on a large number of parameters and, thus, the general definition of a "standard" is virtually impossible. In this work, we conduct a comparative performance study of silicon anode tapes prepared from commercially available materials while using both a well-defined electrode configuration and cycling method. Our results demonstrate that the polymer binder has a profound effect on the cell performance. Furthermore, we show that key parameters such as specific capacity, capacity retention, rate capability, and so forth can be strongly affected by the choice of silicon material, polymer binder and electrolyte system − even the formation of metastable crystalline $Li_{15}Si_4$ is found to depend on the electrode composition and low potential exposure time. Overall, the use of either poly(acrylic acid) with a viscosity-average molecular weight of 450.000 or poly(vinyl alcohol) Selvol 425 in combination with both silicon nanopowder containing a native oxide surface layer of ∼1 nm in diameter and with a monofluoroethylene carbonate-based electrolyte led to improved cycling stability at high loadings.

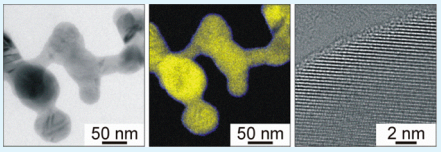

KEYWORDS: *lithium-ion battery, high-capacity anode, polymer binder, electrolyte, silicon, nanoparticles*

INTRODUCTION

Silicon is a promising anode material for future lithium ion and next-generation lithium batteries. This is due in part to both its natural abundance and high theoretical specific capacity of 4008 mA h/g when fully lithiated according to the formation of $Li_{21}Si_5$ or 3340 mA h/g for metastable $Li_{15}Si_4$.[1−4] Compared to graphite, the state-of-the-art anode material in lithium ion batteries with a theoretical specific capacity of 372 mA h/g, silicon appears as a very attractive material to be combined with high-capacity cathodes such as high-energy lithium nickel−cobalt−manganese oxide (HE-NCM), sulfur, and other materials. However, further enhancement in the electrochemical charge storage and the overall energy density of such batteries is necessary to fulfill the requirements imposed by future applications, particularly in the electromobility sector (transport, etc.).[5,6] A stable specific capacity of more than 1000 mA h/g often serves as benchmark for next-generation anodes.[7]

In contrast to graphite, silicon must be regarded as a conversion material. This means that lithium insertion does not occur as an intercalation reaction but rather as a conversion reaction comprising breakup and reorganization of the silicon lattice upon alloying with lithium. In this context, it is important to note that the accommodation of lithium ions is associated with a large volume expansion of up to 300%, whereas graphite only swells by approximately 7% during intercalation.[8] Also, a "fresh" surface is generated during each cycle and, thus, lithium is irreversibly consumed in the electrolyte decomposition and formation of a solid-electrolyte-interface (SEI) layer. For silicon, the formation of a stable SEI, as reported for graphite, is difficult to achieve. However, such anode surface film is crucial for achieving long-term cycling stability and for the working principle of lithium ion batteries per se.[9]

Battery electrodes made from silicon suffer from severe mechanical stress due to the above-mentioned issues. As a result, they often fracture and pulverize after a few charge/discharge cycles. The latter typically leads to both loss of electrical contact of the silicon particles and increase in cell

Received: May 2, 2013
Accepted: July 10, 2013
Published: August 1, 2013

resistance accompanied by rapid capacity fading. In addition, electrolyte decomposition occurs repeatedly which delivers further irreversible capacity during cycling—drying out of the cell cannot be prevented.[7]

In recent years, many efforts have been made aiming to overcome these limitations and difficulties by strongly focusing on novel silicon materials. Both nanostructuring and fabrication of silicon/carbon composites and silicon alloys have been proposed as tools to obtain better control over the volume expansion and surface chemistry with the main objective of preserving the electrode integrity. The preparation of silicon nanowires, nanotubes, core−shell structures, thin films, and the use of chemical vapor deposition (CVD), hydrothermal, and etching processes have proven to deliver promising nanostructured materials.[3,10−20] Moreover, porous electrode morphologies have been shown to buffer volume changes during cycling more effectively than nonporous ones.[21−23] Comparative investigations of various electrolyte additives have also demonstrated that variations in SEI properties such as thickness and flexibility can lead to enhanced electrode performance.[24−29]

The high demands to silicon anodes further require thorough investigations into the influence of other cell and electrode components on the electrochemical performance. The impact of polymer binders on the overall behavior of the complete electrode system, particularly with regard to its mechanical properties and interactions with electrolytes and other active components, is highly relevant for the cycling stability. However, only few literature reports address this issue.[30,31] Nonetheless, the results suggest that the polymer binder itself has the potential to tremendously improve the performance of silicon anodes. Functionality, polarity, viscosity, flexibility, and in some cases, conductivity appear to be the crucial factors.

The viscosity of binder solutions is known to strongly affect both the processing and drying behavior of electrode slurries and, therefore, also the resulting electrode morphology.[32] We note that in some literature reports, the optimization of silicon electrode morphologies has already been examined.[32,33] A novel method to achieving cross-linking of a binder mixture after electrode processing has recently been described. This method led to significant improvement in electrode robustness and to enhanced cycling behavior.[34] Overall, many of these studies suggest that poly(vinylidene fluoride) (PVDF) is not an appropriate binder for silicon-based anodes and should be replaced by water-soluble and more functional binders. For some silicon composites and nanomaterials, PVDF seems to work satisfyingly, however, and for that reason, comparisons with alternative binders are often not shown.

The above makes clear that the performance of silicon electrodes depends on a broad range of different key parameters, including silicon particle size and shape, particle morphology, binder properties, additives, electrode processing and morphology, adhesion to the current collector, active mass fraction, loading, and other factors. Consequently, comparisons of different silicon materials and binders are often difficult to draw because further important parameters may differ significantly. We note that even small changes in the cycling method (i.e., capacity limitations and altering current densities) can lead to different electrode reactions, which in turn, have a profound effect on the overall electrochemical behavior.[2]

To the best of our knowledge, there are no systematic studies described in the literature focusing on commercially available silicon and binder materials employing both a well-defined electrode configuration and cycling method. The present work is dedicated to the analysis of anodes prepared from different binders and silicon nanopowders combined with a thorough structural characterization of the starting materials. Also, different electrolytes were tested in the two-electrode cells with lithium serving as counter electrode. We show that the performance of the electrodes employed here can be significantly altered by properly adjusting single parameters.

EXPERIMENTAL SECTION

Materials. Silicon nanopowders with nominal average particle sizes (APS) of less than 100 and 50 nm were purchased from Aldrich and Alfa Aesar, respectively, and used as received. Poly(acrylic acid) (PAA) with a viscosity-average molecular weight (M_v) of 450.000 g/mol, polyethylene oxide (PEO) with M_v of 400.000 g/mol, carboxy methyl cellulose sodium salt (CMC) with a weight-average molecular weight M_W of 250.000 g/mol and alginic acid sodium salt (AA) of medium viscosity were purchased from Aldrich. Poly(vinyl alcohol) (PVA) Selvol 425 and poly(vinylidene fluoride) (PVDF) Kynar HSV 900 were obtained from Sekisui Chemical Co., Ltd., Japan and Arkema, Colombes, France, respectively. Super C65 carbon black was obtained from Timcal, Bodio, Switzerland. Six-hundred-micrometer-thick lithium foil was purchased from China Energy, Linyi, China and stored in an argon-filled glovebox. Battery grade $LiPF_6$ was obtained from Toyota Tsusho Europe S.A., Dusseldorf, Germany and also stored under argon. Ethylene carbonate (EC) and ethyl methyl carbonate (EMC) were obtained from BASF SE, Ludwigshafen, Germany. Monofluoroethylene carbonate (FEC) was provided by Solvay, Frankfurt, Germany. The water content in the electrolytes was equal to or less than 10 ppm. Seventeen-micrometer-thick copper foil provided by Gould Electronics, Eichstetten, Germany, was used as current collector and glass fiber filter discs (GF/D) from Whatman served as separators.

Methods. Transmission electron microscopy (TEM) and high-resolution TEM (HRTEM) measurements were conducted on an FEI Titan^3 80−300 microscope operated at 300 kV accelerating voltage. This instrument is enclosed in a box to both dampen acoustic disturbances and minimize temperature variations. On the optical axis below the lower pole piece of the objective lens, the microscope is equipped with a so-called C_S image corrector (CEOS, Heidelberg, Germany), which is used to minimize the spherical aberration and other lens aberrations such as coma, higher-order astigmatism, and star aberration.[35] Using this corrector, in HRTEM imaging, the point resolution can be improved to 0.08 nm at 300 kV, which is comparable to the information limit of the imaging system. Images were taken by means of a 2K CCD camera (Gatan UltraScan 1000 P) mounted in an on-axis position. Image recording was done by the Digital Micrograph (Gatan, Munich, Germany) software at an exposure time of 0.5 s. In addition, energy-filtered TEM (EFTEM) was performed using a Gatan Tridiem model 865 ER, which also has a 2K UltraScan CCD camera as detector. Element maps were obtained via the three-window method with typical recording times of several ten seconds per individual image.[36] For drift correction and further image processing such as background extrapolation and subtraction the Digital Micrograph software was used. Scanning electron microscopy (SEM) images were taken on a Zeiss LEO 1530 microscope. X-ray diffraction (XRD) patterns were recorded on a STOE Stadi P in transmission geometry using Cu−Kα radiation and a Dectris (Baden, Switzerland) Mythen strip detector. X-ray photoelectron spectroscopy (XPS) spectra were acquired on a VersaProbe PHI 5000 Scanning ESCA Microprobe from Physical Electronics Ismaning, Germany, with monochromatic Al−K_α X-ray source and a hemispherical electron energy analyzer. The C 1*s* signal from adventitious hydrocarbon at 284.8 eV was used as energy reference to correct for charging. Nitrogen physisorption experiments were conducted at 77 K using the Autosorb-6 automated gas adsorption station from Quantachrome Corporation, Boynton Beach, Florida. The specific surface area was calculated using the Brunauer−Emmett−Teller (BET) model in the relative pressure range from 0.05 to 0.3.

Table 1. Overview of Electrodes Prepared from Different Polymer Binders

binder	silicon nanopowder	electrode thickness (μm)	silicon content (%)	silicon loading (mg/cm^2)	specific capacity (mA h/cm^2)
AA (medium viscocity)	Alfa (laser-synthesized from vapor phase, APS < 50 nm)	30−34	61.4	1.2	4.8
PAA (450.000)	Alfa (laser-synthesized from vapor phase, APS < 50 nm)	22−29	63.8	1.3	5.1
PVA (Selvol 425)	Alfa (laser-synthesized from vapor phase, APS < 50 nm)	29−31	63.1	1.4	5.6
CMC (250.000)	Alfa (laser-synthesized from vapor phase, APS < 50 nm)	36−41	63.6	1.4	5.6
PEO (400.000)	Alfa (laser-synthesized from vapor phase, APS < 50 nm)	30−50	63.6	1.1	4.4
PVDF (Kynar HSV 900)	Alfa (laser-synthesized from vapor phase, APS < 50 nm)	32−44	63.2	1.4	5.6

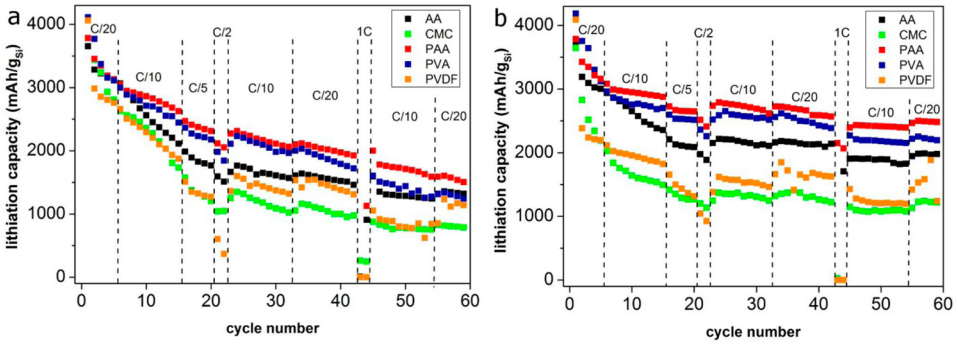

Figure 1. Lithiation (discharge) capacity as a function of cycle number for electrodes comprising different polymer binders. (a) EC-based electrolyte. (b) FEC-based electrolyte. Note that the first cycle capacity of the electrode prepared from CMC is equal to that of the PAA-based electrode and, therefore, superimposed in panel a.

Electrode Processing. Electrodes were fabricated using the slurry coating method. First, silicon nanopowder, carbon black, and polymer binder in aqueous solution (or PVDF in N-ethyl pyrrolidone (NEP)) were added to a beaker and homogenized by planetary mixing using a Thinky (Laguna Hills, California) ARE 200 mixer. The ratio was kept constant in all experiments at 63% silicon, 22% carbon black, and 15% binder if not stated otherwise. This composition was adopted from the work of Kovalenko et al. on AA as binder.[30] We note that the solvent content of the binder solution and the additional amount of solvent added to the slurry mixture was strongly dependent on both the solubility and viscosity of the polymer binder. The slurry was then cast onto the copper foil using the doctor blade method. For this purpose, both a MTV (Cologne, Germany) film applicator and an Erichsen (Hemer, Germany) Coatmaster 510 were utilized. After coating, the electrode tapes were transferred to a vacuum drying chamber at a temperature of 100 °C (120 °C for PVDF/NEP) and dried for 30 min (60 min for PVDF/NEP) under constant nitrogen flow at a pressure of 100 mbar. Thereafter, the electrodes were dried overnight at 1 mbar. The electrode thickness was determined using a Mitutoyo (Mitutoyo Deutschland, Neuss, Germany) film thickness monitor. Lastly, 13 mm diameter discs were punched out using an EL-Cut electrode cutter from EL-CELL (Hamburg, Germany) and introduced into an argon-filled glovebox. Prior to assembling test cells, the electrode discs were evacuated at 100 °C overnight.

Electrochemical Testing. To test the silicon anodes, we assembled two-electrode cells of the coin cell-type in an argon-filled glovebox. Lithium foil (13 mm diameter discs) was used as counter electrode and glass fiber filter discs (17 mm in diameter) were used as separators. The electrolyte solution (250 μL) was 1 M $LiPF_6$ in mixed solvents of EC/EMC (1:1 w/w) or FEC/EMC (1:1 w/w). The cells were cycled at 25 °C in a potential range between 0.005 and 1.0 V vs Li/Li^+ using a MACCOR (Tulsa, Oklahoma) battery cycler. Galvanostatic charge/discharge experiments were carried out at various *C*-rates. The *C*-rate was calculated on the basis of silicon assuming a theoretical specific capacity of 4008 mA h/g. If not stated otherwise, the final voltage was kept constant until a current drop of 80% was reached before starting the subsequent half cycle.

RESULTS AND DISCUSSION

Influence of Polymer Binder. In a first set of experiments, we examined different commercially available polymer binders while keeping other key parameters such as silicon starting material, composition, loading, and so forth as similar as possible. Table 1 summarizes the main parameters of the electrodes studied.

We note that the silicon nanopowder with a nominal APS < 50 nm employed in the experiments was readily dispersible in both water and N-ethyl pyrrolidone and contained only a very thin (≤1 nm) oxide surface layer, as can be seen in Figure 3 below. Top view SEM images of the corresponding anode tapes are shown in Figure S1 in the Supporting Information. The electrodes were cycled at moderate current rates of *C*/20 and *C*/10 to obtain insight into the behavior at virtually complete lithiation and delithiation. However, higher *C*-rates (here *C*/5, *C*/2, and 1*C*) were also tested to examine the performance at comparatively short charging/discharging times.

In the present work, our aim was to exploit the full capacity range of silicon, although a stable specific capacity of approximately 1000 mA h/g is regarded as sufficient for next-generation anodes. Part of the reason for this is that we wanted to find out (1) whether the different polymer binders used are capable of preserving the electrode integrity during maximum volume expansion/contraction of the silicon nanoparticles (in other words, whether they are flexible enough to accommodate the expansion/contraction of the electrode during charge/discharge), and (2) what effect the oxygen layer at the top surface of the nanoparticles has on the total capacity.

dx.doi.org/10.1021/am401642c | ACS Appl. Mater. Interfaces 2013, 5, 7299−7307

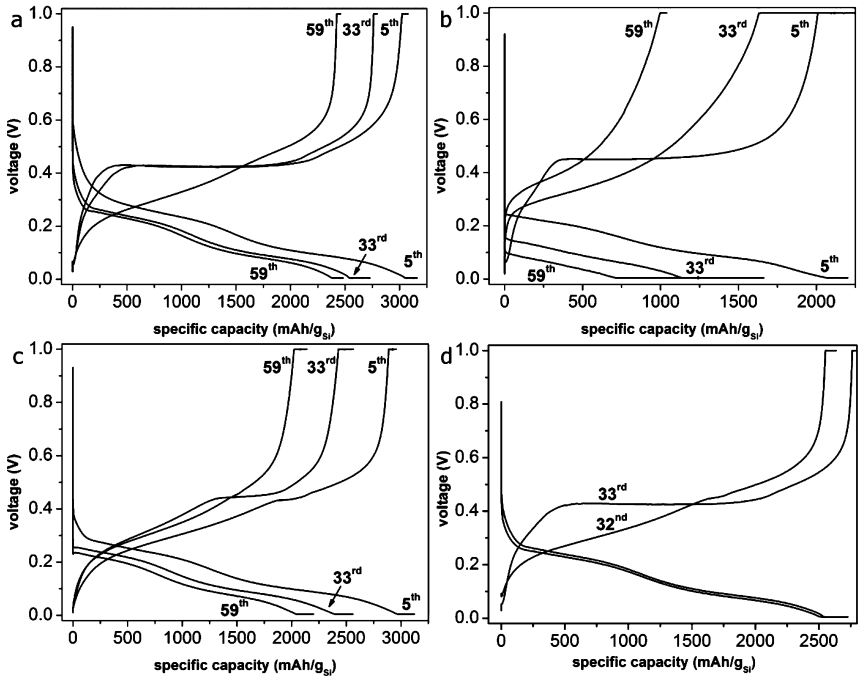

Figure 2. (a–c) Voltage profiles of electrodes prepared from (a) PAA, (b) PVDF, and (c) PVA at a rate of C/20. The electrolyte system used in these experiments was FEC/EMC. Note that only the 5th, 33rd, and 59th cycles are shown. (d) Voltage profiles of the PAA-based electrode for the 32nd (C/10 rate) and 33rd (C/20 rate) cycles.

Figure 1a shows the lithiation (discharge) capacity as a function of cycle number for the EC-based electrolyte. The same data but for the FEC-based electrolyte are shown in Figure 1b. From these plots, it is evident that both the binder and electrolyte have a strong impact on the overall performance. The results obtained with PEO as binder are not shown in Figure 1 because the electrodes revealed a very large capacity drop throughout the course of the first few cycles (see Figure S2 in the Supporting Information). It can be clearly seen that the cycling behavior of cells containing FEC is superior to that of cells running with the EC-based electrolyte. However, independent of the electrolyte, electrodes made from PAA show the best capacity retention, followed by PVA, AA, PVDF, and CMC. For the EC-based electrolyte, the capacity retention among the different binders is similar after approximately 50 cycles. Table S1 in the Supporting Information summarizes the main results for both electrolyte systems, including initial lithiation capacity, first cycle capacity loss, and capacity retention (based on the second cycle lithiation capacity, i.e., after SEI formation) after the 5th, 33rd, 42nd, and 59th cycles at the C/20 rate.

We find that, except for CMC, the use of FEC leads to both slightly higher lithiation capacities and higher irreversible capacities on the first cycle. However, capacity fading in the subsequent cycles is much faster for the EC-based electrolyte. Overall, the electrodes reveal a more stable cycling behavior at higher specific capacities with FEC, which is particularly evident for both PAA and PVA, showing specific lithiation capacities of more than 2600 and 2500 mA h/g, respectively, after 20 cycles. We note that this result is in line with literature reports on the performance enhancement of silicon anodes achieved using FEC-containing electrolytes.[25−28] In recent years, it has been shown that the electrochemical reduction of FEC leads to formation of a thinner, smoother, and more stable SEI accompanied by both decreased cell impedance and enhanced mechanical robustness of the electrode.[25,27] The latter ultimately results in higher reversible capacities and prolonged cycle life.

The overall best performance is achieved using PAA as binder, as can be seen in Figures 1a, b. The irreversible capacities in the first cycle are rather low with 13% and 11% for FEC and EC, respectively. After 59 cycles, 73% of the second cycle lithiation capacity is retained when using the FEC-based electrolyte. This is considerably better than the value of 43% achieved with EC. In addition, we find that the electrodes exhibit fairly good rate capability; the specific capacities are affected only to a limited extend by galvanostatic cycling at higher C-rates such as C/10 and C/5. Even at rates as high as C/2 and 1C the electrodes are capable of delivering more than 2000 mA h/g. PAA thus seems to be an appropriate binder for nanoscale silicon anodes, in agreement with the findings by Magasinski et al. and Komaba et al.[32,37]

In contrast to PAA, PVA has not yet been reported to be a potential binder for silicon anodes. However, PVA has been shown to exhibit interesting dispersion and adhesion properties depending on the degree of polymerization and hydrolysis.[38] The data in Figure 1 indicate that PVA shows in fact promise as polymer binder for silicon anodes. The first cycle irreversible capacities are found to be similar to that of electrodes made from PAA, namely 14 and 10% for FEC- and EC-based electrolytes, respectively. The capacity retention after 59 cycles is 59% (FEC) and 33% (EC), respectively. This result shows that the overall retention rate is lower compared to PAA but still superior to any other polymer binder employed in this work, except AA with EC-based electrolyte.

AA has been reported to exhibit outstanding properties as binder for silicon anodes.[30] This, however, could not be fully confirmed by our experiments, likely because of the fact that several parameters such as silicon starting material, loading, and other factors differed from those in the work of Kovalenko et al.

Here, AA reveals the second best performance with EC-based electrolyte after 59 cycles and the third best performance with FEC when considering the overall capacity retention. The irreversible capacities on the first cycle are found to be higher compared to both PAA and PVA (19% for FEC and 13% for EC). After 59 cycles, the electrodes delivered 62% (FEC) and 40% (EC) of the second cycle lithiation capacity, respectively. However, we note that the capacity fading from the 33rd cycle onward is slower than that observed for silicon anodes made from PVA, and PAA reveals the same trend with FEC-based electrolyte. We find that the capacity decreases by approximately 9% for both AA and PAA and 13% for PVA between the 33rd and 59th cycles when using the FEC-based electrolyte. In contrast, EC leads to capacity losses of 18% for AA, 30% for PAA, and 37% for PVA. These data indicate that AA might be a well-suited binder for silicon anodes to achieve long-term cycling stability. In addition, they clearly show that AA leads to much better electrode performance than both CMC and PVDF, in agreement with the work of Kovalenko et al.[30]

CMC-based electrodes reveal first cycle irreversible capacities of 24% (FEC) and 11% (EC), respectively. The capacity retention after 59 cycles is rather low for both electrolyte systems, namely only 43% (FEC) and 23% (EC), respectively. The electrodes show rapid capacity fading throughout the course of the first 20 cycles but stabilize afterward. This behavior is similar to that observed for AA even though the specific capacities are significantly lower. We note that better performances have already been obtained on the same silicon material but using CMC with M_W of 90.000 g/mol.[28] However, in that work, the silicon content in the electrode was only 40% and the loading per square centimeter was approximately 6 times lower than that here (see Table 1), both of which help to explain the differences.

As in many previous reports, PVDF has not proven to be an appropriate binder for lithium ion battery applications based on silicon as active material.[30,32] The data shown in Figure 1 demonstrate that the electrodes cannot be cycled in a stable manner although the specific capacity is higher than that observed for CMC after 59 cycles. The irreversible capacities observed in the first cycle are very large for both FEC- (43%) and EC-based (29%) electrolytes. Because the same silicon starting material was used for these experiments, this result indicates that PVDF is not capable of preserving the electrode integrity on the first cycle.

The voltage profiles for electrodes made from PAA, PVDF, and PVA measured with FEC-based electrolyte in Figures 2a−c provide further insight into the electrochemical properties. We note that both AA and CMC binders behave rather similar to PAA. For clarity, only the 5th, 33rd, and 59th cycles are shown. From these data, it can be seen that PVDF electrodes reveal a large overpotential before the first lithiation plateau is reached at approximately 0.25 V. Although this behavior is not fully understood yet, we can speculate about the cause: either no conductive framework of carbon black and silicon is obtained from slurry coating or the electrode disintegrates already during the first cycle. The data in Figures 2a−c also indicate significant differences in the delithiation (charge) profiles among the different polymer binders. For both PVDF and PAA, a distinct plateau is observed at approximately 0.45 and 0.425 V, respectively, in the fifth cycle. This plateau can presumably be attributed to the formation of $Li_{15}Si_4$ during the previous discharge. Metastable crystalline $Li_{15}Si_4$ has been reported to form upon lithiation of silicon at low potentials (<50 mV). Delithiation of this compound occurs at a higher potential (overpotential) relative to lithium which is also observed here.[2] For PAA, the plateau remains virtually unchanged up to cycle no. 33. In contrast, it cannot be observed anymore in the case of PVDF. Instead a subtle plateau appears at lower potentials. From these data, we conclude that the suppression of the formation of $Li_{15}Si_4$ is directly related to the degree of electrode degradation because the appearance of this phase apparently requires an adequate degree of lithiation in addition to sufficient exposure time to low potentials.

Figure 2d shows the voltage profiles of the PAA-based electrode for the 32nd and 33rd cycles. The 32nd cycle was conducted at a rate of $C/10$ and does not show a distinct delithiation plateau. However, the plateau appears on the subsequent cycle at the $C/20$ rate, which supports our hypothesis. Interestingly, in contrast to all other binders studied here, electrodes made from PVA reveal no such plateau over the first few cycles. Nevertheless, a comparatively short delithiation plateau can be seen on the 33rd cycle, which vanishes throughout the course of the subsequent cycles (see 59th cycle in Figures 2a, c). The same is also observed for the PAA-based electrode. To our knowledge, such strong impact of polymer binders on the alloying properties of silicon has not been reported yet. The specific interactions of PVA with the silicon nanoparticles seem to suppress the formation of crystalline $Li_{15}Si_4$. As reported by Obrovac et al., the specific capacity of $Li_{15}Si_4$ is 3340 mA h/g and cannot be exceeded once formed. Indeed, only for PVA- and PVDF-based electrodes we find first cycle lithiation capacities greater than 4000 mA h/g (see Table S1 in the Supporting Information). PAA-, AA-, and CMC-based electrodes, by contrast, deliver capacities of less than or equal to 3800 mA h/g on the first discharge, which is indicative of the formation of $Li_{15}Si_4$ in silicon anodes prepared from these binders.

A further indication of the affinity of PVA to both silicon and carbon black is given in the first cycle discharge profile in the voltage range between 1.8 and 0.1 V (see Figure S3 in the Supporting Information).[38] We note that rather similar plateaus related to electrolyte decomposition are found for all the other polymer binders, independent of the electrolyte system used. However, PVA does not show such plateaus neither with the FEC- nor with the EC-based electrolyte. This result suggests that either electrolyte decomposition at the electrode surface occurs at a large overpotential because PVA acts as an insulating layer or that SEI formation proceeds very slowly (superimposed by the lithiation process). From Figures 1a, b and Table S1 in the Supporting Information, it is apparent that the PVA-based electrodes show both a high initial capacity and a comparably low irreversible capacity on the first cycle. However, it can also be seen that the electrodes degrade strongly before reaching a rather stable performance after approximately 10 (FEC) and 20 cycles (EC), respectively. This is particularly evident for the FEC-based electrolyte when compared to electrodes made from PAA, and, therefore, points toward sluggish SEI formation.

In summary, the above results establish that interactions between the binder and the surface of both the silicon and carbon black particles strongly affect the reactions involved in SEI formation as well as the overall electrode behavior on the subsequent charge/discharge cycles. In addition, they show that polymers with a large fraction of polar functional groups such as carboxyl and hydroxyl groups are capable of stabilizing the

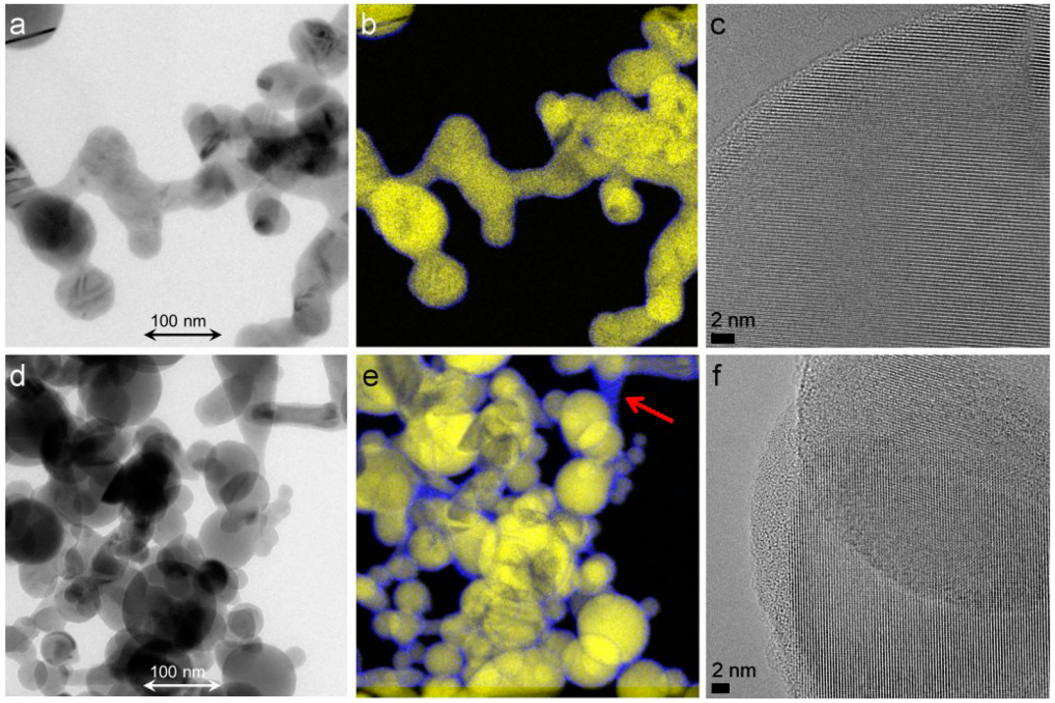

Figure 3. Microstructure of (a–c) Si-50 and (d–f) Si-100 nanopowders. (a, d) Bright-field TEM images. (b, e) EFTEM mapping of the areas shown in panels a and d. The red arrow in panel e indicates an oxygen-rich domain. (c, f) HRTEM images.

active material to a certain extent, which, in turn, is advantageous for electrode processing and performance.

Influence of SiO_x Content. Commercially available silicon materials are typically covered by a native oxide layer and further terminated with hydroxyl groups. During synthesis, such a shell is readily formed because of presence of trace amounts of oxygen and water. As a result, most silicon micro- and nanopowders can be processed under ambient atmosphere because the surface oxide acts as a passivating layer. In particular for silicon nanopowders, the native oxide layer has been reported to strongly influence the electrochemical properties. This is not very surprising because the surface represents a large portion of the entire sample. However, the exact role of the surface oxide and the reactions involved are unclear.[39] For example, it is not known to what extent or under which conditions SiO_x species can be electrochemically reduced by lithium.[39−43] Morita et al. showed that inactive SiO_2 particles in Si-SiO_x-C composites help buffer the volume changes but reduce the reversible capacities.[44] Other groups suggested that the negative effects of SiO_x species in silicon anodes are due to the insulating nature of silicon oxide and lithium silicates that might form during cycling.[39,45,46]

In this work, we studied two different kinds of silicon nanopowders. In addition to the material used in the experiments described above (Alfa Aesar, laser-synthesized from gas phase, APS < 50 nm) we conducted measurements on nanoscale silicon purchased from Aldrich (APS < 100 nm). In the following, we refer to the Alfa and Aldrich nanosilicon as Si-50 and Si-100, respectively. Both materials were characterized by various techniques, including X-ray diffraction (XRD), X-ray photoelectron spectroscopy (XPS), N_2-physisorption, and transmission electron microscopy (TEM). The XRD and XPS data and the N_2-adsorption/desorption isotherms are shown in Figures S4–S6 in the Supporting Information. The average crystallite sizes were determined by applying the Scherrer equation to the line broadening of the most intense peaks. From this analysis, we obtained values of approximately 47 and 78 nm for Si-50 and Si-100, respectively.[47] From XPS, it is apparent that Si-100 contains a much larger fraction of SiO_x species on the surface than Si-50. Deconvolution of the Si 2p spectrum indicates three different silicon bonding states for both materials. These peaks can be assigned to Si^0, Si–O and Si–Cl species. The presence of chlorine is likely related to the production process of the silicon nanopowders. The O 1s data can be fit to two peaks. The main peaks at binding energies of (532.30 ± 0.05) eV and (532.77 ± 0.05) eV for Si-50 and Si-100, respectively, can be attributed to oxygen in SiO_x and the shoulder peaks at (533.89 ± 0.05) eV and (534.28 ± 0.05) eV, respectively, can be assigned to surface hydroxyl groups. Analysis of both oxygen bonding states by comparison of the peak areas reveals a more condensed oxide layer in Si-100, as expected. Surprisingly, the Brunauer–Emmett–Teller (BET) surface areas are very similar for both materials, namely 32 and 35 m^2/g for Si-50 and Si-100, respectively. Although this result is not fully understood, we believe that it might be related to the different degree of polydispersity. As mentioned above, both nanopowders were also analyzed by bright-field TEM, high-resolution TEM (HRTEM), and energy-filtered TEM (EFTEM) to obtain insight into the oxygen content in the particle shell (see Figure 3).

From the bright-field TEM image for Si-50 in Figure 3a, it can be seen that a large fraction of particles forms intergrown aggregates. Therefore, this material contains complex networks of particle assemblies in addition to single nanoparticles of spherical shape. However, the particle size distribution appears to be quite narrow. Only few particles are smaller or larger than 50 and 150 nm, respectively. TEM diffraction–contrast imaging already indicates that the Si-50 material is highly crystalline. This, however, can be more clearly seen in the HRTEM image in Figure 3c. Even though this image shows only one-quarter of

Table 2. Overview of Electrodes Prepared from Different Types of Silicon Nanopowders

binder	silicon nanopowder	electrode thickness (nm)	silicon content (%)	silicon loading (mg/cm^2)	specific capacity (mA h/cm^2)
AA (medium viscocity)	Alfa (laser-synthesized from vapor phase, APS < 50 nm)	30−34	61.4	1.2	4.8
AA (medium viscocity)	Aldrich (APS < 100 nm)	30−35	63.1	1.4	5.6

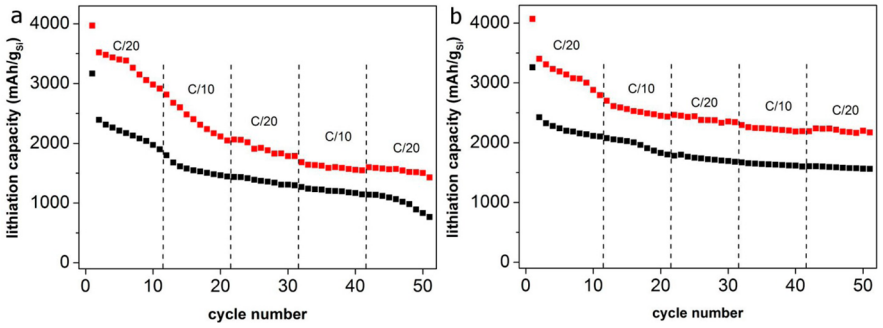

Figure 4. Lithiation (discharge) capacity as a function of cycle number for electrodes prepared from Si-50 (solid squares in red) and Si-100 (solid squares in black) nanopowders and AA as binder. (a) EC-based electrolyte. (b) FEC-based electrolyte.

a single nanoparticle, it reveals the presence of an amorphous surface layer of approximately 1 nm in diameter, hinting to oxide coverage. To prove that, element-specific images were recorded by EFTEM. For this purpose, the silicon distribution was imaged by means of the Si-L_{23} ionization edge at 99 eV and the oxygen map was obtained via the O−K edge (532 eV threshold energy). In both cases, background extrapolation was done using a power-law model. The resulting qualitative Si/O composition map is given in Figure 3b for Si-50. The layer in blue, enveloping particles and assemblies thereof, marks oxygen-rich regions. In addition, this EFTEM image verifies that the presence of an oxygen-containing layer in the interparticle boundaries can be largely ruled out.

In contrast to Si-50, the Si-100 sample is more polydisperse (see Figure 3d). Here, particle sizes ranging from approximately 20 nm to more than 200 nm in diameter are found. Similar to Si-50, this material comprises predominantly particles of spherical shape. Moreover, the Si/O map in Figure 3e shows that a significant number of particles is interconnected through oxygen-rich domains. Such SiO_x domains can extend over large areas, as indicated by the arrow in Figure 3e. In general, the oxygen-containing layer is much thicker, which is in agreement with the results from XPS. This is further confirmed by HRTEM. The image in Figure 3f shows particles with a crystalline core and an amorphous SiO_x shell of several nanometers thickness.

Lastly, electrodes were fabricated from both silicon nanopowders using AA as binder to analyze the influence of the SiO_x content on the overall performance. Table 2 summarizes the main parameters. The capacity vs. cycle charts for the EC- and FEC-based electrolytes are shown in Figure 4. We note that the data obtained on Si-50 cannot be directly compared to those shown in Figure 1 because the cycling program was slightly modified: the final voltage was kept constant until a current drop of 99.9% was reached before starting the subsequent half cycle.

Similar behavior is observed for both electrolyte systems. However, the irreversible capacities in the first cycle are significantly different. The smaller Si-50 silicon material reveals irreversibilities of 20 and 13% for the FEC- and EC-based electrolytes, respectively. In contrast, values of 28% (FEC) and 24% (EC) are found for electrodes made from Si-100. At first glance, this result suggests that SEI formation on the surface of the silicon nanoparticles plays no major role. Rather, consumption of lithium because of formation of inactive lithium oxide and/or silicate species, which may be expected to form in larger quantities in the oxygen-rich Si-100-based anode, appears to be the decisive factor to explain the difference. In both cases, the specific capacity of Si-50 is higher compared to that of Si-100 (by approximately 1000 and 600 mA h/g in the 1st and 50th cycles, respectively). This result can also be explained by the larger amount of SiO_x in the Si-100 sample. Under the cycling conditions used in this study, such SiO_x species seem to be inactive and, further, to impede the lithiation of the active silicon core because of ohmic losses associated with the poor electrical conductivity. However, we note that the silicon content (without SiO_x) in the electrodes was not precisely known due to the surface oxide and, thus, the specific capacities discussed here contain some error. On the basis of the TEM imaging data, the error margin is expected to be quite small for Si-50 (less than 4%). In contrast, for Si-100 the error margin is much larger. However, it can hardly be estimated from TEM as the particle size distribution is much broader compared to that of Si-50 and the oxide surface layer is less defined (e.g., in terms of thickness).

The capacity retention after 50 cycles does not differ much among the samples. Sixty-five percent of the second cycle lithiation capacity is retained when using the FEC-based electrolyte. This is significantly better than the values of 42 and 34% for Si-50 and Si-100, respectively, achieved with EC. We can therefore rule out a positive buffering effect of generated LiO_2, SiO_x, and/or inactive silicate species on the cycling behavior.[39,45,46] Instead, the voltage profiles in Figure 5 show that the lithiation process of Si-100 occurs at lower potentials (higher overpotentials relative to lithium). This is likely not only a result of the different size of the silicon particles but can also be attributed to an increased cell resistance because of the larger oxygen content. Also, the delithiation curves show a more pronounced plateau at approximately 0.425 V for the Si-50-based electrode. As discussed earlier in this paper, this

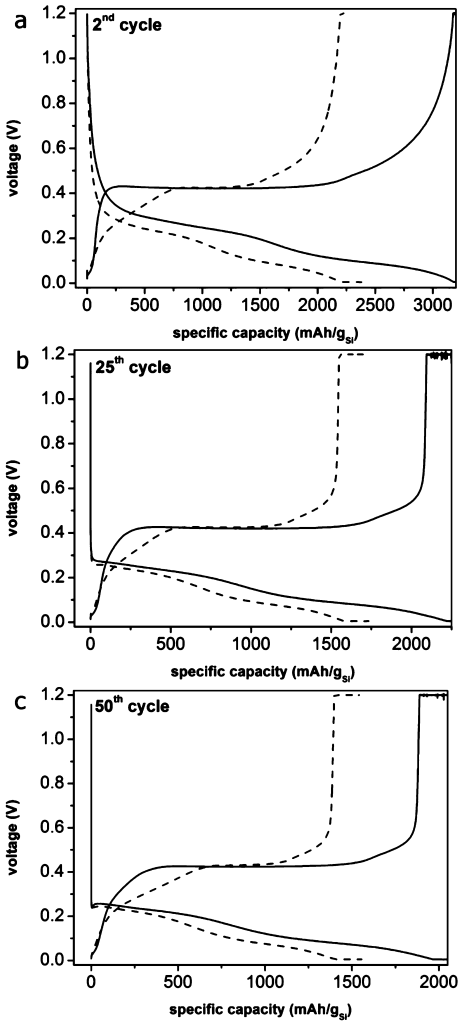

Figure 5. Voltage profiles of electrodes prepared from Si-50 (solid lines) and Si-100 (dashed lines) nanopowders and AA as binder for the (a) 2nd, (b) 25th, and (c) 50th cycles at a rate of C/20. The electrolyte system used in these experiments was FEC/EMC.

plateau can be associated with the formation of crystalline $Li_{15}Si_4$ upon lithiation and indicates that a larger fraction of this highly lithiated phase is formed in the case of Si-50. Overall, these results are in good agreement with the work of Xun et al., in which similar differences in cycling performance were observed.[39] Therein, surface oxide on nanoscale silicon was removed by etching with hydrofluoric acid.

CONCLUSIONS

The development of silicon-based anodes for next-generation lithium ion batteries is a demanding task due to the large volume changes associated with alloying/dealloying of silicon and the resulting capacity fading. In the present work, we have shown that the performance strongly depends on the choice of active material, polymer binder, and electrolyte system. Several commercially available binders have been tested and it turned out that electrodes prepared from poly (acrylic acid) with M_v of 450.000 g/mol exhibit the best cycling stability, followed by poly(vinyl alcohol) Selvol 425, alginic acid sodium salt of medium viscosity, poly(vinylidene fluoride) HSV 900, carboxy methyl cellulose sodium salt with M_w of 250.000 g/mol, and polyethylene oxide with M_v of 400.000 g/mol. The latter three do not show promise as binders for silicon-based anodes because of rapid capacity fading and/or unstable cycling behavior. Overall, the results indicate that particularly polyvinyl binders with a large amount of polar functional groups such as carboxyl, and hydroxyl groups allow for facile electrode processing and, further, are capable of stabilizing the active components which, ultimately, leads to both longer cycle life and higher reversible capacities. In addition, silicon nanopowders with both a narrow size distribution and a thin surface oxide layer are beneficial to achieving high capacities and low first cycle irreversibilities and to keeping the overpotential to a minimum. Positive buffering effects of in situ generated LiO_2 and inactive SiO_x and/or silicate species on the cycling behavior are not observed. Lastly, we note that independent of polymer binder and silicon material, FEC-containing electrolyte systems have the potential to significantly improve the overall performance of silicon anodes.

ASSOCIATED CONTENT

Supporting Information

Additional data from galvanostatic cycling experiments, N_2-physisorption, XRD, XPS, and SEM imaging. This material is available free of charge via the Internet at http://pubs.acs.org.

AUTHOR INFORMATION

Corresponding Author

*E-mail: christoph.erk@kit.edu (C.E.); juergen.janek@kit.edu (J.J.). Phone: +49 721 608-26870 (C.E.); +49 721 608-28827 (J.J.).

Author Contributions

C.E. and R.S.: experimental work and data analysis. T.B., H.S., and J.J.: project planning and data analysis. The manuscript was written by C.E. and T.B. All authors have given approval to the final version of the manuscript.

Notes

The authors declare no competing financial interest.

ACKNOWLEDGMENTS

We thank Hauke Metelmann and Christoph Weidmann for assistance in XPS and N_2-physisorption measurements. This study is part of projects being funded within the BASF International Network for Batteries and Electrochemistry. C.E., T.B., H.S., and J.J. work at the Battery and Electrochemistry Laboratory BELLA, which is cofinanced by Karlsruhe Institute of Technology (KIT) and BASF SE.

REFERENCES

(1) Obrovac, M. N.; Christensen, L. *Electrochem. Solid-State Lett.* **2004**, *7*, A93−A96.
(2) Obrovac, M. N.; Krause, L. J. *J. Electrochem. Soc.* **2007**, *154*, A103−A108.
(3) Chan, C. K.; Peng, H. L.; Liu, G.; McIlwrath, K.; Zhang, X. F.; Huggins, R. A.; Cui, Y. *Nat. Nanotechnol.* **2008**, *3*, 31−35.
(4) Hatchard, T. D.; Dahn, J. R. *J. Electrochem. Soc.* **2004**, *151*, A838−A842.
(5) Armand, M.; Tarascon, J. M. *Nature* **2008**, *451*, 652−657.
(6) Etacheri, V.; Marom, R.; Elazari, R.; Salitra, G.; Aurbach, D. *Energy Environ. Sci.* **2011**, *4*, 3243−3262.
(7) Kasavajjula, U.; Wang, C. S.; Appleby, A. J. *J. Power Sources* **2007**, *163*, 1003−1039.
(8) Key, B.; Bhattacharyya, R.; Morcrette, M.; Seznec, V.; Tarascon, J. M.; Grey, C. P. *J. Am. Chem. Soc.* **2009**, *131*, 9239−9249.
(9) Yen, Y. C.; Chao, S. C.; Wu, H. C.; Wu, N. L. *J. Electrochem. Soc.* **2009**, *156*, A95−A102.

(10) Chan, C. K.; Patel, R. N.; O'Connell, M. J.; Korgel, B. A.; Cui, Y. *ACS Nano* **2010**, *4*, 1443−1450.
(11) Chen, H. T.; Xu, J.; Chen, P. C.; Fang, X.; Qiu, J.; Fu, Y.; Zhou, C. W. *ACS Nano* **2011**, *5*, 8383−8390.
(12) Choi, N. S.; Yao, Y.; Cui, Y.; Cho, J. *J. Mater. Chem.* **2011**, *21*, 9825−9840.
(13) Cui, L. F.; Ruffo, R.; Chan, C. K.; Peng, H. L.; Cui, Y. *Nano Lett.* **2009**, *9*, 491−495.
(14) Gohier, A.; Laik, B.; Kim, K. H.; Maurice, J. L.; Pereira-Ramos, J. P.; Cojocaru, C. S.; Van, P. T. *Adv. Mater.* **2012**, *24*, 2592−2597.
(15) Yoo, H.; Lee, J. I.; Kim, H.; Lee, J. P.; Cho, J.; Park, S. *Nano Lett.* **2011**, *11*, 4324−4328.
(16) Li, X. L.; Meduri, P.; Chen, X. L.; Qi, W.; Engelhard, M. H.; Xu, W.; Ding, F.; Xiao, J.; Wang, W.; Wang, C. M.; Zhang, J. G.; Liu, J. *J. Mater. Chem.* **2012**, *22*, 11014−11017.
(17) Magasinski, A.; Dixon, P.; Hertzberg, B.; Kvit, A.; Ayala, J.; Yushin, G. *Nat. Mater.* **2010**, *9*, 353−358.
(18) Datta, M. K.; Maranchi, J.; Chung, S. J.; Epur, R.; Kadakia, K.; Jampani, P.; Kumta, P. N. *Electrochim. Acta* **2011**, *56*, 4717−4723.
(19) Hu, Y. S.; Demir-Cakan, R.; Titirici, M. M.; Muller, J. O.; Schlogl, R.; Antonietti, M.; Maier, J. *Angew. Chem., Int. Ed. Engl.* **2008**, *47*, 1645−1649.
(20) Richman, E. K.; Kang, C. B.; Brezesinski, T.; Tolbert, S. H. *Nano Lett.* **2008**, *8*, 3075−3079.
(21) Ge, M. Y.; Rong, J. P.; Fang, X.; Zhou, C. W. *Nano Lett.* **2012**, *12*, 2318−2323.
(22) Rong, J. P.; Masarapu, C.; Ni, J.; Zhang, Z. J.; Wei, B. Q. *ACS Nano* **2010**, *4*, 4683−4690.
(23) Guo, J.; Sun, A.; Wang, C. *Electrochem. Commun.* **2010**, *12*, 981−984.
(24) Chen, L. B.; Wang, K.; Xie, X. H.; Xie, J. Y. *J. Power Sources* **2007**, *174*, 538−543.
(25) Etacheri, V.; Haik, O.; Goffer, Y.; Roberts, G. A.; Stefan, I. C.; Fasching, R.; Aurbach, D. *Langmuir* **2012**, *28*, 965−976.
(26) Dalavi, S.; Guduru, P.; Lucht, B. L. *J. Electrochem. Soc.* **2012**, *159*, A642−A646.
(27) Choi, N. S.; Yew, K. H.; Lee, K. Y.; Sung, M.; Kim, H.; Kim, S. S. *J. Power Sources* **2006**, *161*, 1254−1259.
(28) Lin, Y. M.; Klavetter, K. C.; Abel, P. R.; Davy, N. C.; Snider, J. L.; Heller, A.; Mullins, C. B. *Chem. Commun.* **2012**, *48*, 7268−7270.
(29) Nakai, H.; Kubota, T.; Kita, A.; Kawashima, A. *J. Electrochem. Soc.* **2011**, *158*, A798−A801.
(30) Kovalenko, I.; Zdyrko, B.; Magasinski, A.; Hertzberg, B.; Milicev, Z.; Burtovyy, R.; Luzinov, I.; Yushin, G. *Science* **2011**, *334*, 75−79.
(31) Liu, G.; Xun, S. D.; Vukmirovic, N.; Song, X. Y.; Olalde-Velasco, P.; Zheng, H. H.; Battaglia, V. S.; Wang, L. W.; Yang, W. L. *Adv. Mater.* **2011**, *23*, 4679−4683.
(32) Han, Z. J.; Yabuuchi, N.; Shimomura, K.; Murase, M.; Yui, H.; Komaba, S. *Energy Environ. Sci.* **2012**, *5*, 9014−9020.
(33) Guo, J. C.; Wang, C. S. *Chem. Commun.* **2010**, *46*, 1428−1430.
(34) Koo, B.; Kim, H.; Cho, Y.; Lee, K. T.; Choi, N. S.; Cho, J. *Angew. Chem., Int. Ed. Engl.* **2012**, *51*, 8762−8767.
(35) Uhlemann, S.; Haider, M. *Ultramicroscopy* **1998**, *72*, 109−119.
(36) Egerton, R. F. *Electron Energy-Loss Spectroscopy in the Electron Microscope*, 2nd ed.; Plenum Press: New York, 1996; Section 5.3.6: Core-Loss Images and Elemental Mapping, p 330−334.
(37) Magasinski, A.; Zdyrko, B.; Kovalenko, I.; Hertzberg, B.; Burtovyy, R.; Huebner, C. F.; Fuller, T. F.; Luzinov, I.; Yushin, G. *ACS Appl. Mater. Interfaces* **2010**, *2*, 3004−3010.
(38) Ryu, M.; Kim Y. M.; Oh, E. S.; Yang, S. R.; Kim, J.; Chun, Lee, C. H.; Lee, K. Y.; Lee, S. J.; Jin, J. M.; Kim, T. U.S. Patent 0 264 568, 2007.
(39) Xun, S.; Song, X.; Wang, L.; Grass, M. E.; Liu, Z.; Battaglia, V. S.; Liu, G. *J. Electrochem. Soc.* **2011**, *158*, A1260−A1266.
(40) Graetz, J.; Ahn, C. C.; Yazami, R.; Fultz, B. *Electrochem. Solid-State Lett.* **2003**, *6*, A194−A197.
(41) Huang, H.; Kelder, E. M.; Chen, L.; Schoonman, J. *J. Power Sources* **1999**, *81*, 362−367.
(42) Saint, J.; Morcrette, M.; Larcher, D.; Laffont, L.; Beattie, S.; Peres, J. P; Talaga, D.; Couzi, M.; Tarascon, J. M. *Adv. Funct. Mater.* **2007**, *17*, 1765−1774.
(43) Guo, B. K.; Shu, J.; Wang, Z. X.; Yang, H.; Shi, L. H.; Liu, Y. N.; Chen, L. Q. *Electrochem. Commun.* **2008**, *10*, 1876−1878.
(44) Morita, T.; Takami, N. *J. Electrochem. Soc.* **2006**, *153*, A425−A430.
(45) Jung, Y. S.; Lee, K. T.; Oh, S. M. *Electrochim. Acta* **2007**, *52*, 7061−7067.
(46) Philippe, B.; Dedryvere, R.; Gorgoi, M.; Rensmo, H.; Gonbeau, D.; Edstrom, K. *Chem. Mater.* **2013**, *25*, 394−404.
(47) Nanda, J.; Kuruvilla, B. A.; Sarma, D. D. *Phys. Rev. B* **1999**, *59*, 7473−7479.